Journal of ELECTRONIC MATERIALS, Vol. 48, No. 11, 2019
https://doi.org/10.1007/s11664-019-07521-y

Thermoelectric Properties of $In_2O_3(ZnO)_k$ (k = 3, 4, 5, 7) Superlattice Ceramics

SHUHUI LI,[1] YING ZHOU,[1] LIJUN CUI,[1] ZHENHUA GE,[1,2] and JING FENG[1,3]

1.—Faculty of Materials Science and Engineering, Kunming University of Science and Technology, Kunming 650093, China. 2.—e-mail: zge@kmust.edu.cn. 3.—e-mail: jingfeng@kmust.edu.cn

$In_2O_3(ZnO)_k$ superlattice ceramics are promising oxide thermoelectric materials, as superlattice interfaces are effective in scattering phonons and filtering low-energy electrons to decrease thermal conductivity and improve the figure of merit (ZT) value. In this work, homologous compounds were prepared by solid-state reaction method using ZnO and In_2O_3 as raw materials. Phase purity and crystal structure were characterized by x-ray diffraction, revealing that $In_2O_3(ZnO)_k$ crystallizes in an R3 m space group for odd k values and $P6_3/mmc$ for even k values. The study of thermoelectric (TE) properties showed that as k increased, the thickness of $InO(ZnO)_3^+$ also increased, while the electrical conductivity, thermal conductivity, Seebeck coefficient, power factor and ZT value were all decreased. $In_2O_3(ZnO)_3$ samples obtained a maximum power factor of 651 $\mu W\ m^{-1}\ K^{-2}$ at 973 K, and also achieved a maximum ZT value of 0.24 at 973 K.

Key words: $In_2O_3(ZnO)_k$ ceramic, thermoelectric properties, natural superlattice

INTRODUCTION

Energy is an important foundation for economic development. Since the second industrial revolution, the world has been keeping up with an ever-increased demand of electricity, with an ever-increasing consumption of fossil fuels. However, fossil fuels are not renewable, Fortunately, thermal energy is considered renewable, because it is ubiquitous and inevitable. Most energy in our daily life is generated by thermal processes, whereas the energy we waste is primarily and ultimately in the form of heat.[1,2] Thermoelectric (TE) technology is one of the most important methods that can be applied to realize high-efficiency heat-to-electricity energy conversion. It is thus especially important to develop thermoelectric materials which can be applied at high temperatures for power generation applications.[3] TE materials have been intensively studied during the last few decades. However, the energy conversion efficiency is relatively low, which limits the application of TE devices as promising alternative energy sources.[4] The efficiency of TE materials is determined by the dimensionless figure of merit (ZT), defined as:

$$ZT = (\alpha^2\sigma/\kappa)T \quad (1)$$

where σ and κ are the electrical and thermal conductivity, respectively, α is the Seebeck coefficient, and T is the absolute temperature. Among various TE materials, inorganic semiconductors, particularly those with a narrow bandgap like Si-based materials,[5,6] intermetallics,[7] chalcogenides,[8] half-Heusler alloys,[9,10] and Zintl compounds,[11] are the most investigated objects. However, these materials exhibit disadvantages, such as rigorous preparation conditions, which need to be carried out under certain gas protection. Besides, the application temperature of the abovementioned materials is relatively low, and they contain heavy metals,

(Received February 21, 2019; accepted August 2, 2019; published online August 12, 2019)

which can have associated toxicities. Oxide TE materials possess the following unique advantages: no oxidation problems, stable high-temperature performance; no toxic chemical elements, no human toxicities and environment friendly; simple preparation process; little or no rare metal elements, and are economically feasible. Therefore, oxide TE materials can be applied as high-temperature TE power generators based on their unique advantages.[12]

$In_2O_3(ZnO)_k$ (k is an integer) ceramics are one of the most investigated high-temperature TE materials because of their natural superlattice structure, consisting of InO_2^- layers interleaved with $(InZnk)O_{k+1}^+$ layers along the c axis. These homologous compounds belong to the space group $R3\ m$ for odd k values and $P6_3/mmc$ for even k values (Fig. 1).[18] Natural superlattices, which are the thermodynamically favored phases, possess high-temperature coarsening-resistant and stable nanoscale interfaces. $In_2O_3(ZnO)_k$-based superlattice compounds, which consist of In_2O_3 and ZnO, are some of the best transparent conducting and electronic materials, and have attracted considerable research interest.[13–18] It has been reported that phonons are effectively scattered by an $In_2O_3(ZnO)_k$ natural superlattice interface, as it contains a single atomic InO_2^- layer. The strong phonon scattering source results in low thermal conductivity and a high ZT value for $In_2O_3(ZnO)_k$. The layered nature is thought to impart a low thermal conductivity to the structure, as this behavior has been observed in high-ZT p-type Na-based and Ca-based cobalt oxide systems.[19] Anisotropic superlattice structures can improve ZT values by taking advantage of sharp electron density of states function, due to the quantum confinement effect for Seebeck coefficient and frequent interface scattering of the phonons for thermal transport.[20–24]

To date, studies on the $In_2O_3(ZnO)_k$ system have mainly confirmed films, which can be used in solar cells, and bulk ceramics, which can be used in TE materials at high temperatures. In some reports, ZnO-In_2O_3 films, which can be used as transparent electrodes, have been successfully prepared by radio-frequency (RF) magnetron sputtering. These ZnO-In_2O_3 films have high thermal stability, chemical stability and relatively high electrical conductivity. It has been suggested that these ceramics can be used as TE materials at high temperatures.[25,26] K. Koumoto reported on the TE properties of ZnO and In_2O_3 mixtures synthesized by reaction sintering at 1823 K under air for 2 h.[27] Since then, many researchers have improved the ZT value of $In_2O_3(ZnO)_k$ by introducing dopant atoms and changing chemical components (such as the concentration of indium). Additionally, much effort has been devoted to studying the crystal structure of $In_2O_3(ZnO)_k$. Kazeoka et al. tried to improve the TE properties of $In_2O_3(ZnO)_5$ by partially substituting yttrium for indium, as the maximum Z value was 1.1–1.3 $\times$ 10^{-4} K^{-1} (960–1100 K), which was obtained when Y content was 3%.[28] Al-doped $In_2O_3(ZnO)_5$ was prepared using a classic ceramic procedure by S. Bernik, and the ZT values are very close to that of undoped $In_2O_3(ZnO)_5$ (ZT = 0.01). At the optimal doping amount of Al of 0.05, the ZT value will decrease with an increase in Al content (i.e., when it is higher than 0.05).[29] It is widely accepted that $In_2O_3(ZnO)_k$ natural superlattice structure can be formed under certain thermal conditions, which was first reported by Cannard and Tilley.[29] The results showed that the structures of $(ZnO)_mIn_2O_3$ (m = 4–5, 9, and 11) consist of metal/oxygen layers perpendicular to the c-axis of a hexagonal crystal system.[30] The space group of $In_2O_3(ZnO)_m$ was R3 m when m was odd, and it was $P6_3/mmc$ when m was even. Weissenberg photographs are taken of all $In_2O_3(ZnO)_m$ (m = 3, 4 and 5) single crystals to determine their lattice constants and possible space groups.[31] Masuda has studied the structures of $(ZnO)_5In_2O_3$ and $(ZnO)_5(In_{0.8}Y_{0.2})_2O_3$ using an x-ray diffraction (XRD) Rietveld refinement technique on the basis of the space group R3 m.[32] It was found that the basic structure consists of InO_2^- and

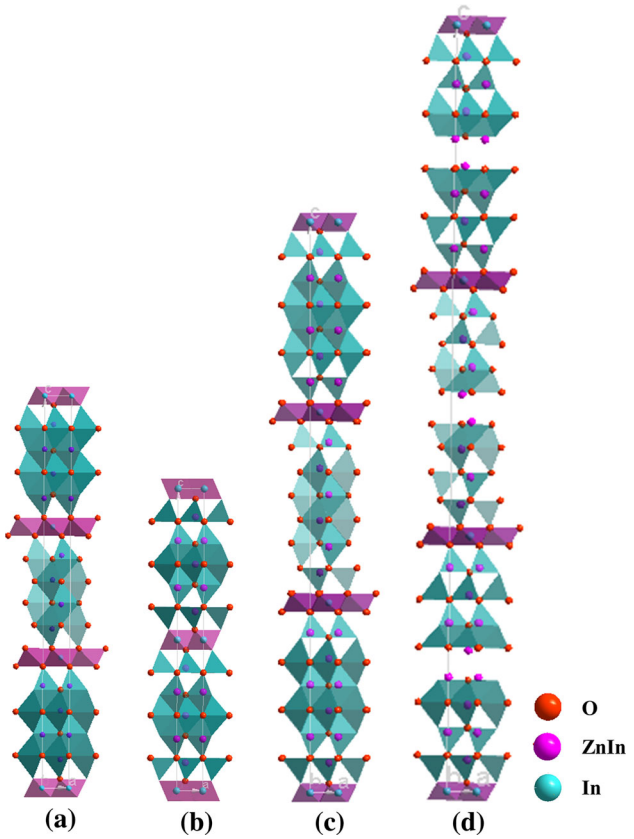

Fig. 1. Crystal structure of $In_2O_3(ZnO)_k$ (k = 3, 4, 5, 7); (a) $In_2O_3(ZnO)_3$; (b) $In_2O_3(ZnO)_4$; (c) $In_2O_3(ZnO)_5$; (d) $In_2O_3(ZnO)_7$.

$(InZn_5)O^{6+}$ layers alternately stacked in alternating layers along the c-axis.

In general, there is a tendency to introduce impurities to improve TE performance and to explore their structural composition unilaterally, but little research has been conducted on the relationship between crystal structure and performance of the $In_2O_3(ZnO)_k$ system. Therefore, in this work, we synthesized $In_2O_3(ZnO)_k$ (k = 3, 4, 5, 7) ceramics using solid-state reaction and performed a series of measurements, including XRD, scanning electron microscopy (SEM), transmission electron microscopy (TEM), Seebeck coefficient (α), thermal conductivity (κ) and Raman spectroscopy, to characterize the prepared $In_2O_3(ZnO)_k$ samples.

EXPERIMENTAL SECTION

Homologous compounds of $In_2O_3(ZnO)_k$ (k = 3, 4, 5, 7) were synthesized by conventional solid-state reaction using starting powders ZnO (Aladdin, 99.99%) and In_2O_3 (Aladdin, 99.99%). Materials with a stoichiometric ratio were subsequently ball-milled (5 h, 300 r/min) with anhydrous ethanol. The solution was then transferred to a conical flask and was kept at 70°C for 12 h in an oven under air to dry. The resulting powders were ground and sieved through 300 meshes to obtain well-distributed powers, which were later pressed into compact discs of 15 mm in diameter under a pressure of 3 MPa for 2 min. The discs were transferred into an alumina crucible and sintered at 1474–1623 K for 2 h.

Phase purity and crystal structure were characterized by XRD (Cu-Kα Bruker D8, Germany) and the bulk density of the pellets was determined by Archimedes method. The samples were coated with a thin layer of gold for microstructure observations, which were performed on a scanning electron microscope (ZEISS, EVO 18-21-57). A transmission electron microscope (FEI Tecnai G2 F20, 200 kV, USA) was used to examine the microstructures of the as-prepared samples. Raman spectra of the superlattice were collected using a LabRAM Aramis Raman system (Horiba Jobin Yvon, Edison, NJ, USA). The bandgap of $In_2O_3(ZnO)_k$ (k = 3, 4, 5 and 7) superlattice was calculated using the Kubelka–Munk formula based on the test results of an ultraviolet–visible–near-infrared (UV–VIS-NIR) spectrophotometer (SHIMADZU-UV-3600Plus). The electrical conductivity and Seebeck coefficient were measured using a commercial ZEM-3 device (Ulvac-Riko, Japan) in a partial atmosphere of helium. The thermal conductivity was calculated according to the expression, $\kappa = DC_P\rho$ where D, C_p *and* ρ are thermal diffusivity coefficient, specific heat capacity and density, respectively. The thermal diffusivity coefficient (D) was measured by laser flash diffusivity method in a NETZSCH LFA 457 system.

RESULTS AND DISCUSSION

Phase Purity and Crystal Structure

The phase purity and crystal structure of the superlattice ceramics were investigated by x-ray diffraction (XRD). Figure 2 shows that XRD patterns of the as-prepared samples of $In_2O_3(ZnO)_3$, $In_2O_3(ZnO)_4$, $In_2O_3(ZnO)_5$ and $In_2O_3(ZnO)_7$ are consistent with standard PDF cards PDF#20-1439, PDF#20-1438, PDF#20-1440 and PDF#20-1441, respectively. For the $In_2O_3(ZnO)_4$ sample, XRD patterns can be indexed using a hexagonal symmetry, while for $In_2O_3(ZnO)_3$, $In_2O_3(ZnO)_5$ and $In_2O_3(ZnO)_7$, a rhombohedral symmetry was needed to include all the diffraction peaks. This work proves that $In_2O_3(ZnO)_k$ compounds crystallize in space group R3 m for odd k values and $P6_3/mmc$ for even k values.[18] The lattice parameters of rhombohedral symmetry can be determined using the following equation:

$$a(R) = \frac{1}{3}\sqrt{3a(H)^2 + c(H)^2} \tag{2}$$

where $a(H)$ and $c(H)$ are the lattice constants for the hexagonal phase structure. These lattice constants can be calculated using the following relationship[33,34]:

$$\frac{1}{d^2} = \frac{4}{3}\left(\frac{h^2 + hk + k^2}{a(H)^2}\right) + \frac{l^2}{c(H)^2} \tag{3}$$

All the lattice constants are listed in Table I, and all of these values also show good consistency with the reported data.[18]

Figure 3 shows the SEM photograph of $In_2O_3(ZnO)_k$ (k = 3, 4, 5, 7) ceramic bulks after sintering at 1473–1623 K. In all cases, the grain size of each sample was several microns due to repeated calcination of raw materials at elevated temperature. In other words, all of their particles have sharp edge features, and their layered structure can be envisioned according to their surface terraces as represented by yellow arrows in the SEM images.

Microstructures of homologous compounds were further analyzed using TEM. Figure 3e shows the TEM image of a representative region for the surface of $In_2O_3(ZnO)_3$ ceramics. It can be seen from the figure that there are obvious contrasting bright and dark alternating periodic stripes on the sample surface, which proves the existence of superlattice structure in this series of ceramics. Figure 3f shows the selected area electron diffraction (SAED), in which the band axis is $2\bar{1}\bar{1}0$, indicating that $In_2O_3(ZnO)_k$ has a single-crystal hexagonal wurtzite structure and its growth direction is 0001. The satellite spot between the two main spots in the pattern is clearly visible, which is a

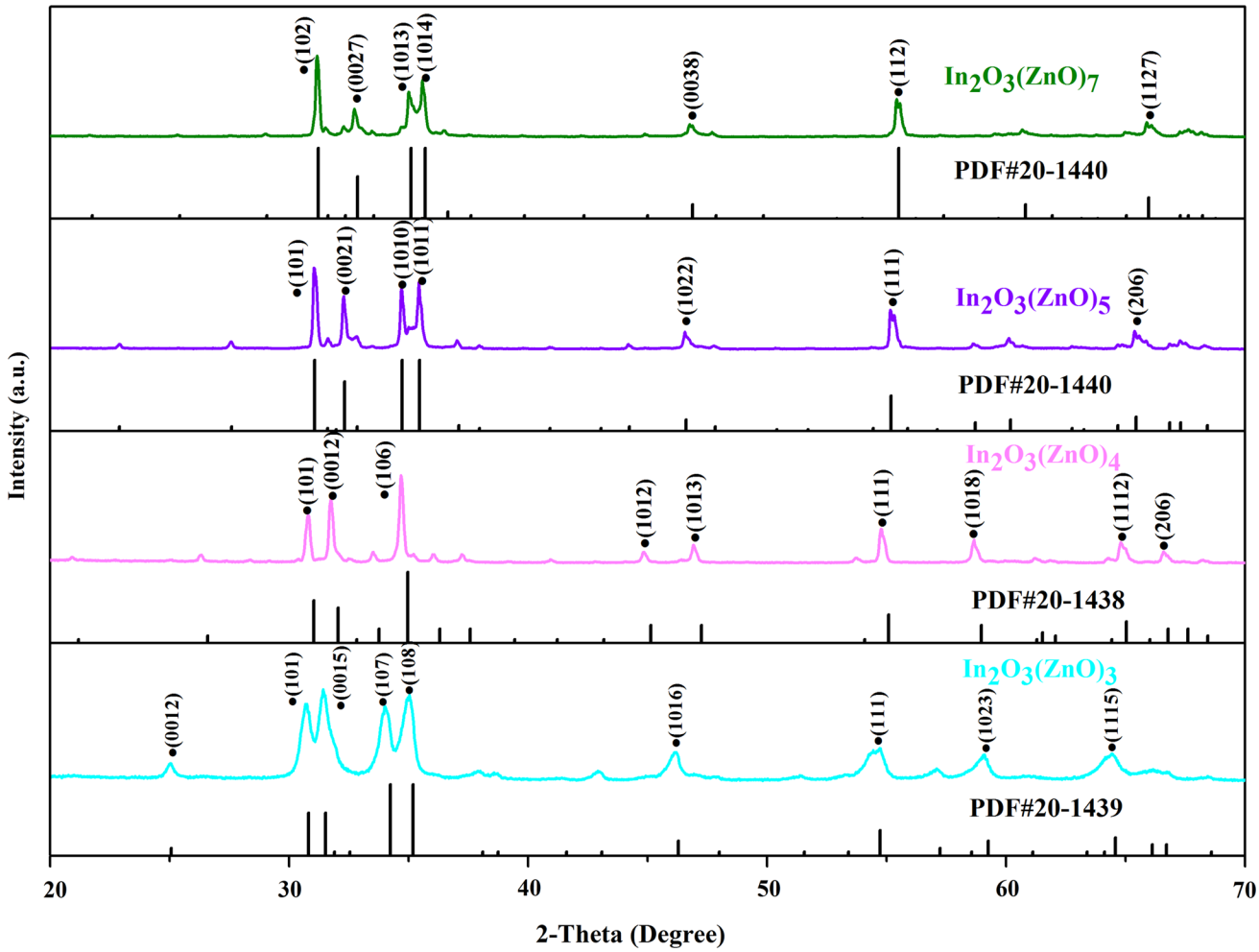

Fig. 2. X-ray diffraction patterns of $In_2O_3(ZnO)_k$ (k = 3, 4, 5, 7) ceramics.

Table I. Space group (SG), lattice parameters (a, b, c/Å), unit cell volume (V/Å^3), bandgap (BG/eV) experimental density (ED/gcm^{-3}), theoretical density (TD/gcm^{-3}) and relative density (RD/%) of $In_2O_3(ZnO)_k$ (k = 3, 4, 5 and 7) ceramics

Sample	SG	$a = b$	c	V	BG	ED	TD	RD
$In_2O_3(ZnO)_3$	R3 m	3.355	42.52	414.49	2.3288	5.939	6.28	94.57
$In_2O_3(ZnO)_4$	$P6_3/mmc$	3.3361	33.544	323.33	2.3317	5.767	6.20	93.02
$In_2O_3(ZnO)_5$	R3 m	3.3330	58.275	560.65	2.3366	5.579	6.11	91.31
$In_2O_3(ZnO)_7$	R3 m	3.33107	73.730	699.88	2.3396	5.442	6.04	90.09

typical feature of modulation structure. Figure 3g shows the high-resolution TEM (HRTEM) image with bright layers of In–O (marked by yellow lines), dark layers of In/Zn–O and In/Zn–O stacks (indicated by the yellow double arrows) sandwiched between adjacent In–O layers. In^{3+} ions in the In–O layer occupy the edge's shared octahedral sites, while the rest of In^{3+} and Zn^{2+} in the In/Zn–O blocks randomly occupy tetrahedral and trigonal/bipyramidal sites. For the homologous compounds of $In_2O_3(ZnO)_k$ (k = integer), when the distance between two adjacent In–O layers is d (Å), there is a linear relationship between d and k[31]:

$$d = 6.349 + 2.602k \quad (4)$$

According to the HRTEM image, the distance d is 1.416 nm, and k = 3 is obtained by substituting the above equation, thereby demonstrating that $In_2O_3(ZnO)_k$ ceramics crystallize in a superlattice structure.

Raman spectroscopy is an important means of analyzing the crystal structure of a substance, as Raman spectroscopy is more sensitive in characterizing the change of crystal structure and chemical bonds than XRD. The information of molecular vibrations in a sample can be obtained by Raman

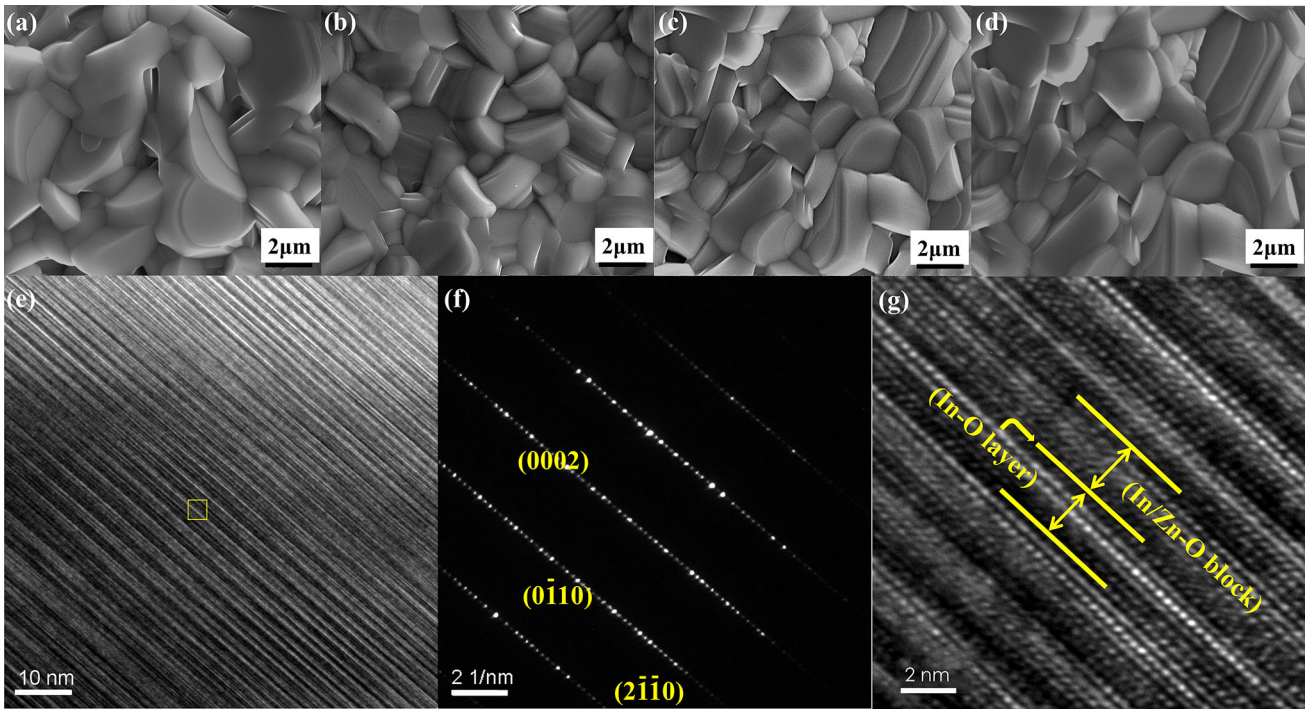

Fig. 3. SEM images of $In_2O_3(ZnO)_3$ (a), $In_2O_3(ZnO)_4$ (b), $In_2O_3(ZnO)_5$ (c), $In_2O_3(ZnO)_7$ (d); low-resolution TEM image of $In_2O_3(ZnO)_3$ ceramic sample (e); elected-area electron diffraction (SAED) pattern of the region of $In_2O_3(ZnO)_3$ ceramic (f); high-resolution TEM (HRTEM) image of $In_2O_3(ZnO)_3$ ceramic (g).

spectroscopy. Figure 4a shows the Raman spectra of $In_2O_3(ZnO)_k$ (k = 3, 4, 5, 7) ceramic bulk materials after sintering at 1473–1623 K. The pure Raman spectra of ZnO and In_2O_3 are shown as a comparison. From Fig. 4a, it can be seen that the Raman spectra of different samples indicate obvious vibration patterns in the 100–700-cm^{-1} range. The red line corresponds to pure ZnO Raman spectra. It is the first-order E_{2high} scattering mode of ZnO at 436 cm^{-1} and the second-order phonon scattering mode at 331 cm^{-1}, which are characteristic Raman peaks for ZnO. The In_2O_3 spectra (yellow line spectrum) shows the expected vibrational modes at 109 cm^{-1}, 135 cm^{-1}, 307 cm^{-1}, 366 cm^{-1}, 495 cm^{-1}, 517 cm^{-1} and 630 cm^{-1}, which in turn clearly demonstrated the In_2O_3 square ferromanganese cubic structure. In contrast to pure ZnO and In_2O_3, $In_2O_3(ZnO)_k$ (k = 3, 4, 5, 7) Raman spectra become flat at about 100 cm^{-1} to about 700 cm^{-1} as the k value decreases. The almost invariant density of phonon states was given, and its "glassy" or quasi-continuous density was demonstrated. $In_2O_3(ZnO)_k$ ceramics were characterized by resonant and non-resonant Raman spectra as well as low-frequency Raman spectra. The vibrational properties of $In_2O_3(ZnO)_k$ exhibited several features of the superlattice structure. It is known that the existence of the superlattice structure of $In_2O_3(ZnO)_k$ was clarified by TEM and XRD results. The superlattice in the Raman spectra periodically depends on the folding and acoustic phonon activation in the Brillouin zone. The bandgap reduction was caused by hybridization of multiple quantum wells and the selective resonance of Fröhlich interactions in $(ZnO)_k$ layers. The vibrational spectra at 520 cm^{-1} and 620 cm^{-1} represented new Raman scattering modes. The 620-cm^{-1} Raman peak was due to the stretching of the In–O bond. As the k value increased, the Raman peak around 620 cm^{-1} shifted from 624 cm^{-1} to 613 cm^{-1}, and a blue shift occured. Due to the smaller the k value, the thickness of In/Zn–O block in the sample decreased and the bandgap increased.

The bandgap of $In_2O_3(ZnO)_k$ (k = 3, 4, 5 and 7) superlattice was calculated using the Kubelka–Munk formula based on the results of UV–VIS–NIR spectrophotometer[35]:

$$F(R) = (1-R)^2 \Big/ 2R \tag{5}$$

where R is the reflectance. It can be seen from Fig. 4 that the bandgap values of $In_2O_3(ZnO)_k$ (k = 3, 4, 5 and 7) were relatively close, being 2.328 eV (k = 3), 2.331 eV (k = 4), 2.336 eV (k = 5) and 2.339 eV (k = 7), which were significantly lower than that of pure ZnO (3.37 eV) and In_2O_3 (3.60 eV). The unit

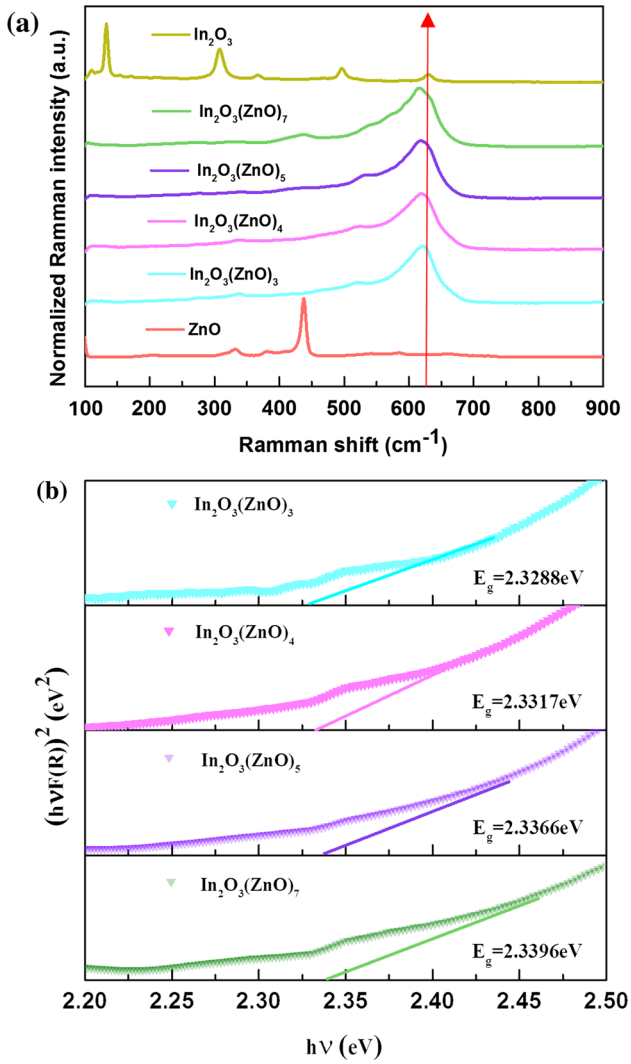

Fig. 4. Raman spectra of $In_2O_3(ZnO)_k$ (k = 3, 4, 5 and 7) superlattices, with pure ZnO and In_2O_3 shown as a reference (a) and Tauc plot between Eg optical bandgap versus $[h\upsilon F(R)]^2$ of $In_2O_3(ZnO)_k$ (k = 3, 4, 5 and 7) (b).

cell parameters and bandgap values of prepared samples are shown in Table I. Obviously, compared to pure In_2O_3 and ZnO, the prepared samples have reduced bandgap values and this result is consistent with the Raman spectral analysis results. This is also consistent with the wide bandgap mentioned above as a high-temperature TE material.

Thermoelectric Properties

The temperature dependence of electrical conductivity σ and Seebeck coefficient α for $In_2O_3(ZnO)_k$ (k = 3, 4, 5 and 7) ceramics are presented in Fig. 5. The electrical conductivity of homologous $In_2O_3(ZnO)_k$ decreased gradually with the increasing temperature, indicating metallic conduction takes place first. In addition, electrical conductivity significantly decreases at room temperature with an increasing k value, which was attributed to the intrinsic properties of $In_2O_3(ZnO)_k$. In general, the number of electrons contributing to the electrical conduction, i.e. carrier concentration, was larger for the smaller k according to the recent literatures.[29,36,37] When conduction electrons in the homologous compounds were injected into the In–O layer, In^{3+} ions were reduced and In–O distances were elongated. Therefore, as k decreases, the increase in In–O distance was related to the enhancement in electrical conductivity.

The Seebeck coefficient trend of k was always negative, which was entirely opposite to that of the electrical conductivity, indicating that all the as-prepared specimens were n-type semiconductors and the major carriers were electrons. The Seebeck coefficient was proportional to the scattering factor and inversely proportional to the carrier concentration ($\alpha \approx \gamma - \ln n$), where γ is the scattering factor, n is the carrier concentration. The value of $|\alpha|$ was proportional to γ and n inversely. The increase of Seebeck coefficient was mainly attributed to the increase of scattering factor, due to the presence of oxygen vacancies in the superlattice layered structure of $In_2O_3(ZnO)_k$ which will cause electron scattering. In addition, the interlaminar thickness of $In_2O_3(ZnO)_3$ was smaller, its bandgap being the narrowest, and the electron scattering increased with the increasing temperature.

As seen in Fig. 5c, the power factor decreased with an increase in k. $In_2O_3(ZnO)_3$ possesses the best performance, which was higher than other samples. The highest power factor (651 μW m^{-1} K^{-2}) has been obtained for k = 3 at 973 K.

Figure 5d shows the temperature dependence of the thermal conductivity calculated from specific heat capacity, thermal diffusivity and bulk density. The thermal conductivity contributes to the lattice (or phonon) thermal conductivity κ_l and electric thermal conductivity κ_e, as written in the expression below:

$$\kappa = \kappa_l + \kappa_e \tag{6}$$

Lattice thermal conductivity κ_l is so sensitive to microstructure, which offers opportunities for reducing κ_l and therefore enhancing TE performance by structure engineering.[38] The incorporation of In_2O_3 into ZnO constitutes a layered superlattice structure, and its interface is a single atomic In–O layer, which strongly scatters phonons and drastically reduces the thermal conductivity. The thermal conductivity κ for each sample gradually decreased with the increasing temperature, proving that phonon scattering played an important role.

As shown in Fig. 6a, the ZT values of all samples increase with increasing temperature, while it decreased with an increase in k. The ZT value was obtained by coupling the three parameters of

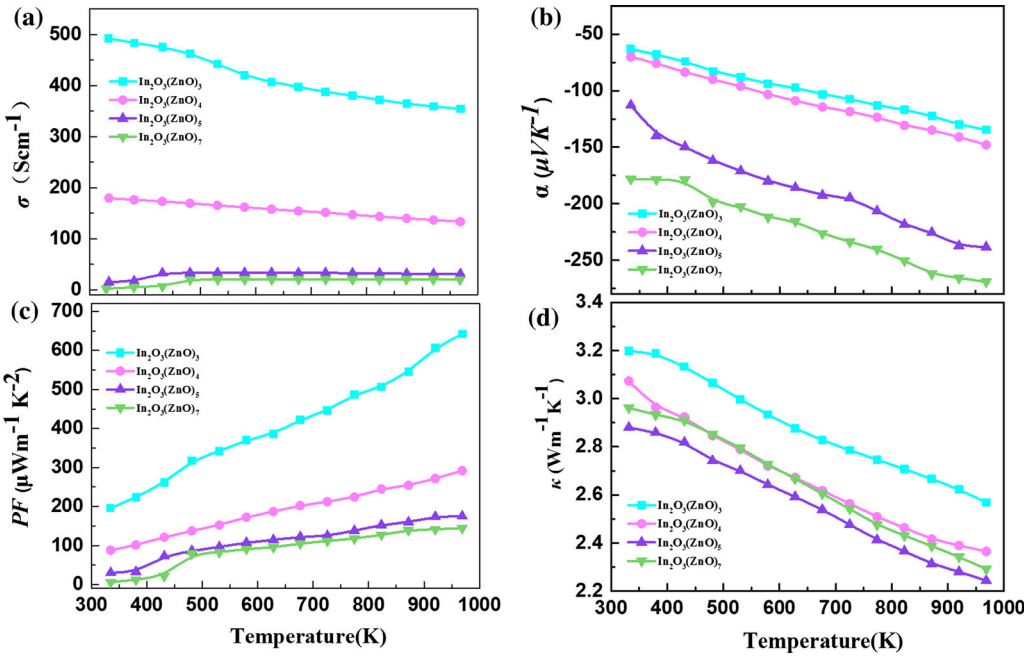

Fig. 5. Temperature dependence of (a) electrical conductivity, (b) Seebeck coefficient, (c) power factor and (d) thermal conductivity for $In_2O_3(ZnO)_k$ (k = 3, 4, 5, 7) superlattice ceramics.

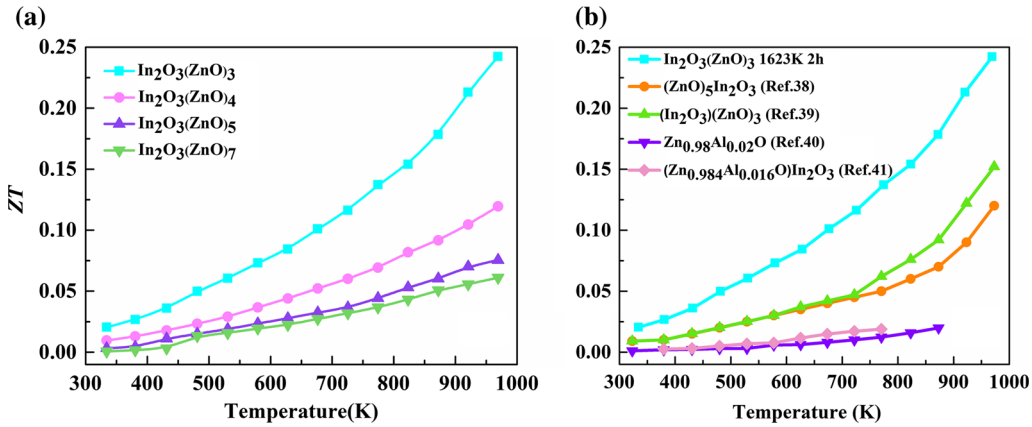

Fig. 6. Temperature dependence of ZT value (a) and the ZT value comparison of this work and other In_2O_3-ZnO system (b).

conductivity, Seebeck coefficient and thermal conductivity. Although the thermal conductivity of $In_2O_3(ZnO)_3$ was lower than the rest, its ZT is the highest due to its high power factor. Figure 6b shows the figure of merit of this work compared with other In_2O_3-ZnO system.[39,40] In this work, the pure $In_2O_3(ZnO)_3$ phase achieved a maximum ZT value of 0.24, and the sample was prepared by solid-state reaction at 1623 K for 2 h. As can be seen from Fig. 6b, the same composition of $In_2O_3(ZnO)_3$ has been reported to have a maximum ZT value of about 0.16, which is lower compared with 0.24 because the differences in experimental process from our work. When k = 5, compared with k = 3, the electrical conductivity decreases because the thickness of In/Zn–O block increases, and causes a relatively low ZT value. In general, the experimental process and composition have an impact on the performance of the samples. $In_2O_3(ZnO)_3$ in this work has a pure phase, and high relative density make its properties more brilliant. So this work provides strong evidence for our selection of fine materials for optimization and makes $In_2O_3(ZnO)_3$ an excellent candidate for further research and optimization for high-temperature TE applications.

CONCLUSIONS

In this paper, the traditional solid-state sintering method was used to successfully prepare $In_2O_3(ZnO)_k$ (k = 3, 4, 5, 7) bulk ceramic materials. Based

on phase structure and microstructure analysis, $In_2O_3(ZnO)_k$ (k = 3, 4, 5, 7) ceramics were layered superlattice structures. The superlattice structures of all samples were formed by alternate stacking of InO_2^- octahedral layers and $InO(ZnO)_3^+$ layers along the c-axis. With an increase of k, the thickness of $InO(ZnO)_3^+$ gradually increased. For $In_2O_3(ZnO)_k$ (k = 3, 4, 5, 7) ceramics, the space group was assigned as R3 m when k is an odd number (k = 4) and as $P6_3/mmc$ when k is an even number (k = 3, 5, 7). An $In_2O_3(ZnO)_3$ sample obtained a maximum power factor of 651 $\mu W\ m^{-1}\ K^{-2}$ and a maximum ZT value of 0.24 at 973 K, which was found to be a huge potential candidate material for high-temperature TE energy conversion.

ACKNOWLEDGMENTS

This work was supported by the National Natural Science Foundation of China (Grant No. 51501086) and Yunnan Provincial Applied Basic Research Projects (Grant No. 2017FA023).

AUTHOR CONTRIBUTIONS

The manuscript was written through contributions of all authors. All authors have given approval to the final version of the manuscript. Shuhui Li and Ying Zhou contributed equally to this work.

REFERENCES

1. C. Forman, I.K. Muritala, R. Pardemann, and B. Meyer, *Renew. Sust. Energ. Rev.* 57, 1568 (2016).
2. J. He and T.M. Tritt, *Science* 357, eaak9997 (2017).
3. T.M. Tritt and M.A. Subramanian, *MRS Bull.* 31, 188 (2006).
4. A. Shakouri, *Ann. Rev. Mater. Res.* 41, 399 (2011).
5. A.I. Hochbaum, R.K. Chen, R.D. Delgado, W.J. Liang, E.C. Garnett, M. Najarian, A. Majumdar, and P.D. Yang, *Nature* 451, 163 (2008).
6. A. I. Boukai, Y. Bunimovich, J. Tahir-Kheli, J. K. Yu, W. A. Goddard and J. R. Heath, Nature **168** (2011).
7. G.J. Snyder, M. Christensen, E. Nishibori, T. Caillat, and B.B. Iversen, *Nat. Mater.* 3, 458 (2004).
8. L.D. Zhao, G.J. Tan, S.Q. Hao, J.Q. He, Y.L. Pei, H. Chi, H. Wang, S.K. Gong, H.B. Xu, V.P. Dravid, C. Uher, G.J. Snyder, C. Wolverton, and M.G. Kanatzidis, *Science* 351, 141 (2016).
9. C.G. Fu, T.J. Zhu, Y.T. Liu, H.H. Xie, and X.B. Zhao, *Energy Environ. Sci.* 8, 216 (2015).
10. C.G. Fu, S.Q. Bai, Y.T. Liu, Y.S. Tang, L.D. Chen, X.B. Zhao, and T.J. Zhu, *Nat. Commun.* 6, 8144 (2015).
11. E.S. Toberer, C.A. Cox, S.R. Brown, T. Ikeda, A.F. May, S.M. Kauzlarich, and G.J. Snyder, *Adv. Funct. Mater.* 18, 2795 (2008).
12. K. Koumoto, Y.F. Wang, R.Z. Zhang, A. Kosuga, and R. Funahashi, *Annu. Rev. Mater. Res.* 40, 363 (2010).
13. K. Nomura, H. Ohta, K. Ueda, T. Kamiya, M. Hirano, and H. Hosono, *Science* 300, 1269 (2003).
14. J.L.F. Da Silva, Y. Yan, and S.H. Wei, *Phys. Rev. Lett.* 100, 255501 (2008).
15. A. Walsh, J.L.F. Da Silva, Y. Yan, M.M. Al-Jassim, and S.H. Wei, *Phys. Rev. B* 79, 073105 (2009).
16. Y.F. Yan, J.L.F. Da Silva, S.H. Wei, and M. Al-Jassim, *Appl. Phys. Lett.* 90, 261904 (2007).
17. H.W. Peng, J.H. Song, E.M. Hopper, Q.M. Zhu, T.O. Mason, and A.J. Freeman, *Chem. Mater.* 24, 106 (2011).
18. C.A. Hoel, T.O. Mason, J.F. Gaillard, and K.R. Poeppelmeier, *Chem. Mater.* 22, 3569 (2010).
19. K. Park, W. S. Seo, K.U. Jang and K. Y. Ko, International Conference on Thermoelectrics **106** (2005).
20. M.S. Dresselhaus, G. Chen, M.Y. Tang, R. Yang, H. Lee, D. Wang, Z. Ren, J.P. Fleurial, and P. Gogna, *Adv. Mater.* 19, 1043 (2007).
21. P. Pichanusakorn and P. Bandaru, *Mater. Sci. Eng. R-Rep.* 67, 19 (2010).
22. Y. Mune, H. Ohta, K. Koumoto, T. Mizoguchi, and Y. Ikuhara, *Appl. Phys. Lett.* 91, 192105 (2007).
23. S.Y. Ren and J.D. Dow, *Phys. Rev. B* 25, 3750 (1982).
24. G. Chen, *Phys. Rev. B* 57, 14958 (1998).
25. H. Ohta, W.S. Seo, and K. Koumoto, *J. Am. Ceram. Soc.* 79, 2193 (1996).
26. H. Hiramatsu, H. Ohta, W.S. Seo, and K.J. Koumoto, *J. Jpn. Soc. Powder Powder Metall.* 44, 44 (1997).
27. M. Kazeoka, H. Hiramatsu, W.S. Seo, and K. Koumoto, *J. Mater. Res.* 13, 523 (1998).
28. M. Košir, M. Čeh, C.W. Ow-Yang, E. Guilmeau, and S. Bernik, *J. Am. Ceram. Soc.* 100, 3712 (2017).
29. P.J. Cannard and R.J.D. Tilley, *J. Solid State Chem.* 73, 418 (1988).
30. N. Kimizuka, M. Isobe, and M. Nakamura, *J. Solid State Chem.* 116, 170 (1995).
31. W. Pitschke and K. Koumoto, *Powder Diffr.* 14, 213 (1999).
32. A. Kadhim, A. Hmood, and H.A. Hassan, *Mater. Sci. Semicond. Process.* 26, 379 (2014).
33. A. Kadhim, A. Hmood, and H.A. Hassan, *Mater. Sci. Semicond. Process.* 15, 549 (2012).
34. T.S. West, W.W. Wendlandt and H.G. Hecht, Wiley, 408 (1967).
35. Y. Orikasa, N. Hayashi, and S. Muranaka, *J. Appl. Phys.* 103, 2229 (2008).
36. E. Guilmeau, D. Berardan, C. Simon, A. Maignan, B. Raveau, D.O. Ovono, and F. Delorme, *J. Appl. Phys.* 106, 053715 (2009).
37. M. Amani, I.M. Tougas, O.J. Gregory, and G.C. Fralick, *J. Electron. Mater.* 42, 114 (2013).
38. S. Bernik, M. Košir, and E. Guilmeau, *Zaštita. Materijala* 57, 318 (2016).
39. C. Dreßler, R. Löhnert, J. Gonzalez-Julian, O. Guillon, J. Töpfer, and S. Teichert, *J. Electron. Mater.* 45, 1459 (2016).
40. T. Endo, J. Fukushima, Y. Hayashi, and H. Takizawa, *Mater. Sci. Forum* 761, 27 (2013).